POLITECNICO DI TORINO
Repository ISTITUZIONALE

Role of defects in the thermal droop of InGaN-based light emitting diodes

Original
Role of defects in the thermal droop of InGaN-based light emitting diodes / De Santi, C.; Meneghini, M.; La Grassa, M.; Galler, B.; Zeisel, R.; Goano, Michele; Dominici, Stefano; Mandurrino, Marco; Bertazzi, Francesco; Robidas, D.; Meneghesso, G.; Zanoni, E.. - In: JOURNAL OF APPLIED PHYSICS. - ISSN 0021-8979. - STAMPA. - 119:9(2016), p. 094501. [10.1063/1.4942438]

Availability:
This version is available at: 11583/2637642 since: 2017-05-04T11:56:59Z

Publisher:
American Institute of Physics Inc.

Published
DOI:10.1063/1.4942438

Terms of use:

This article is made available under terms and conditions as specified in the corresponding bibliographic description in the repository

Publisher copyright
AIP postprint/Author's Accepted Manuscript e postprint versione editoriale/Version of Record

(Article begins on next page)

27 April 2024

Role of defects in the thermal droop of InGaN-based Light Emitting Diodes

C. De Santi[1,*], M. Meneghini[1], M. La Grassa[1], B. Galler[2], R. Zeisel[2], M. Goano[3], S. Dominici[3], M. Mandurrino[3], F. Bertazzi[3], D. Robidas[3,4], G. Meneghesso[1], E. Zanoni[1]

[1]Department of Information Engineering, University of Padova, via Gradenigo 6/B, Padova, 35131, Italy

[2]OSRAM Opto Semiconductors GmbH, Leibnizstrasse 4, 93055 Regensburg, Germany

[3]Department of Electronics and Telecommunications, Politecnico di Torino, corso Duca degli Abruzzi 24, Torino, 10129, Italy

[4]CSIR-SRF, Crystal Growth Centre, Anna University, Chennai-600025, Tamilnadu, India)

This paper reports an investigation of the physical origin of the thermal droop (the drop of the optical power at high temperatures) in InGaN-based light-emitting diodes (LEDs). We critically investigate the role of various mechanisms including Shockley-Read-Hall recombination, thermionic escape from the quantum well, phonon-assisted tunneling and thermionic trap-assisted tunneling; in addition, to explain the thermal droop, we propose a closed-form model which is able to accurately fit the experimental data by using values extracted from measurements and simulations and a limited set of fitting parameters. The model is based on a two-step phonon-assisted tunneling over an intermediate defective state, corrected in order to take into account the pure thermionic component at zero bias and the field-assisted term.

* carlo.desanti@dei.unipd.it, matteo.meneghini@dei.unipd.it

I. INTRODUCTION

Light-emitting diodes (LEDs) are commonly considered as promising devices for all applications requiring high-efficiency light generation, including general lighting, automotive and biomedical applications. In order to approach the high-power end of the illumination market, the overall efficiency of the systems has to be improved at device and circuit level.

A high degree of effort has been put into the understanding of the efficiency droop, i.e. the drop of the optical power at higher bias levels.[1–3] However, there is another mechanism that can severely limit the optical power of InGaN LEDs, namely the thermal droop. This effect consists of the decrease in optical power with increasing temperature, and may lead to a remarkable quenching in the electroluminescence signal. Thermal droop has been reported by several research groups,[4–7] but no rigorous analysis on its physical causes has been carried out up to now. A clear understanding of the physical origin of thermal droop is necessary, since commercial devices are now rated for very high maximum junction temperatures (up to 175 °C), which may lead to a severe optical power drop (up to 25% at 150 °C for typical commercial devices).[8] Preliminary studies tentatively ascribed the thermal droop to Shockley-Read-Hall (SRH) recombination[9] or to carrier escape from the quantum wells;[10] however, the individual contribution of these mechanisms to the luminescence quenching still has to be quantitatively investigated.

The aim of this paper is to improve the understanding of the thermal droop in InGaN-based LEDs by investigating the possible impact of Shockley-Read-Hall recombination, thermionic escape from the quantum well, phonon-assisted tunneling (PAT) and thermionic trap-assisted tunneling (TTAT). By combined experimental and theoretical investigation (i) we demonstrate that – in the samples under investigation – none of these processes alone can explain the temperature dependence of the experimental data over a wide temperature range. To explain the physical origin of the thermal droop, (ii) we propose a novel model based on a thermionic trap-assisted tunneling process which causes the escape of carriers from the quantum wells; the model was validated by using the data on defect density and concentration obtained through capacitance deep level transient spectroscopy (C-DLTS), and information on the energetic structure of the quantum wells derived by numerical simulations.

II. THERMAL DROOP AND DEFECT DENSITY

The devices under test are InGaN-based single quantum well (SQW) light-emitting diodes with different point defect densities, as estimated by DLTS measurements. In the following, we will refer to them as device families A to E. Details on device properties and fabrication processes can be found in

Ref. 11,12. The LEDs under test were grown on a silicon substrate on the c-direction by means of metal-organic vapor phase epitaxy (MOVPE). Over the substrate, a low-temperature AlN nucleation layer was deposited. The epitaxial structure is composed of a 5 µm thick AlGaN/GaN buffer, a highly Si-doped GaN current spreading layer and a single 3 nm thick quantum well. A Mg-doped AlGaN blocking layer and a p-doped GaN:Mg contact layer form the p-side of the device.

In order to quantitatively evaluate the thermal droop, we carried out - on all families - a temperature-dependent characterization of the output power at different current levels. The results of this analysis are summarized in Fig. 1 for 200 µA bias. As can be noticed, the devices lose more than 99% of their light emission at very small current densities when temperature is increased from 83 K to 475 K. This effect is more severe in devices with higher densities of SRH (Shockley-Read-Hall) lattice defects, as revealed by DLTS measurements (see Fig. 2). This result suggests a correlation between the thermal droop and the density of defects responsible for non-radiative recombination. This is also confirmed by the fact that the samples with higher non-radiative SRH recombination coefficient A (evaluated by means of differential lifetime measurements, an entirely independent set of measurements[13]) have the strongest thermal droop (Fig. 2). The extrapolated values of A are comparable to similar reports in the literature.[1,13,14]

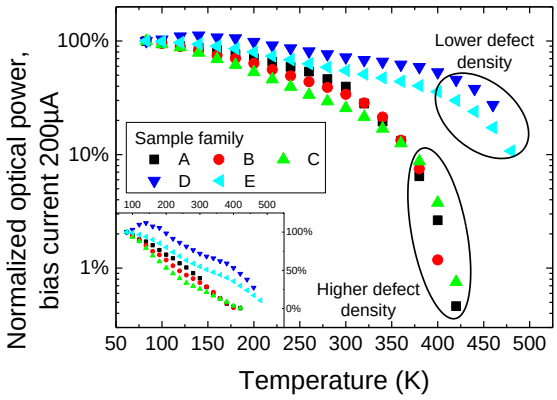

Fig. 1 : Normalized optical power as a function of temperature for all device families under analysis, at a bias current = 200 µA. The different defect densities are indicated.

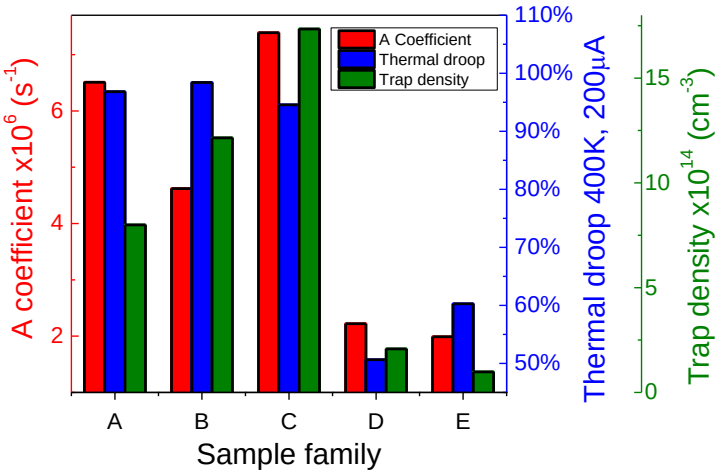

Fig. 2 : Correlation between the SRH A coefficient, obtained by differential lifetime measurements, the trap density evaluated by capacitance DLTS and the amount of thermal droop.

III. SRH RECOMBINATION

To our knowledge, results on the correlation between defect density and thermal droop have been reported only by Wang *et al.*[15] and by Chhajed *et al.*[16] In the paper by Wang *et al.*[15], the authors qualitatively assumed that the thermal droop was caused by the increase in SRH non-radiative recombination with increasing temperature. In the second paper[16], the authors carried out a quantitative analysis based on the SRH rate equation. They derived an explanation based on the non-linear relation between the internal quantum efficiency (IQE) and the non-radiative lifetime (τ_{NR}) due to the presence of the radiative lifetime term (τ_R): IQE= τ_{NR} / (τ_R + τ_{NR}). Their study is based on the assumption that τ_R is constant over the temperature range under analysis, which may be in disagreement with other reports.[17–20] In the following, we will present three different arguments indicating that – in the analyzed temperature range – thermal droop can not be explained by simply taking into account the increase in SRH recombination at high temperature levels. Other factors will be then considered in the subsequent part of the paper.

A. Numerical simulations

To understand if SRH recombination alone can explain our thermal droop data, we carried out numerical simulations in order to evaluate the expected optical power decrease due to non-radiative recombination events. The drift-diffusion model is composed by Poisson's equation and two continuity equations

$$\nabla \cdot \vec{J}_n = q\frac{\partial n}{\partial t} + R_{tot} \qquad \nabla \cdot \vec{J}_p = -q\frac{\partial p}{\partial t} - R_{tot} \tag{1}$$

The constitutive equations for the electron and hole current densities $\vec{J}_n, \vec{J}_p$ include a drift and a diffusion term

$$\vec{J}_n = qn\mu_n\vec{\mathrm{E}} + qD_n\frac{\partial n}{\partial x} \qquad \vec{J}_p = qp\mu_p\vec{\mathrm{E}} - qD_p\frac{\partial p}{\partial x} \tag{2}$$

were μ_n, μ_p are the electron and hole mobilities, $\vec{\mathrm{E}}$ is the electric field, D_n, D_p are the carrier diffusivities. R_{tot} represents the sum of all recombination contributions: Auger, SRH and radiative recombination.

$$R_{tot} = R_{SRH} + R_{RAD} + R_{AUG} \tag{3}$$

Our interest is focused on the modeling of the SRH recombination rate (R_{SRH}), which is expected to be dominant at low currents. In the following, Auger recombination rate (R_{AUG}) has been modeled as

$$R_{AUG} = \left(C_n n + C_p p\right)\left(np - n_i^2\right) \tag{4}$$

Radiative recombination rate (R_{RAD}) has been modeled according to the $\boldsymbol{k}\cdot\boldsymbol{p}$ approach, within the quantum well region, and according to

$$R_{RAD} = B\left(np - n_i^2\right) \tag{5}$$

elsewhere. The variation of B at different temperatures was considered according to $B(T) = B(300)\,[300/T]^{N/2}$.[21] The $\boldsymbol{k}\cdot\boldsymbol{p}$ model parameters used for our simulations are taken from Ref. 22 and are summarized in Table I.

TABLE I. Simulation parameters for k·p model of radiative recombination within the quantum well.

Parameter	GaN	InN	Units
A	3.1892	3.5446	Å
c	5.185	5.718	Å
E_g at T = 0 K	3.507	0.735	eV
α	0.909	0.245	meV K^{-1}
B	830	624	K
X	4.07	5.9272	eV
Δ_{so}	14	1	meV
Δ_{so}	19	41	meV
εr	9.5	15	-
$m_{e\parallel}$	0.20	0.065	-
$m_{e\perp}$	0.20	0.065	-
A_1	−6.56	−8.21	-
A_2	−0.91	−0.68	-

A_3	5.65	7.57	-
A_4	−2.83	−5.23	-
A_5	−3.13	−5.11	-
A_6	−4.86	−5.96	-
D_1	−3.0	−3.0	eV
D_2	3.6	3.6	eV
D_3	8.82	8.82	eV
D_4	−4.41	−4.41	eV
D_5	−4.0	−2.33	eV
D_6	−5.0770	−0.3536	eV
C_{11}	390	271	GPa
C_{12}	145	124	GPa
C_{13}	106	92	GPa
C_{33}	398	224	GPa
C_{44}	105	46	GPa
P_{sp}	−0.034	−0.042	C m^{-2}

The radiative recombination rate inside the active region is usually expressed as a summation running over *j* conduction states, and *i* valence states[23,24]:

$$R_{RAD} = \left(\frac{2\pi}{\hbar}\right)\sum_{i,j}\int\int\left(\frac{\hbar\omega q^2}{2m_0\varepsilon\omega^2}\right)\left|M_{ij}\right|^2\left(f_j - f_i\right)D(E)\rho_{ij}^0 h\left(\hbar\omega - E_{ij}^0\right)dk\,dE \qquad (6)$$

where $D(E)$ is the optical mode density, M_{ij} is the momentum matrix element, $f_i$and f_i are Fermi statistics for *i*-th and *j*-th energy levels, ρ_{ij}^0 is the 2D density of states, and E_{ij}^0 is the energy distance between the two levels. In our simulations, the net SRH recombination rate is calculated as[25]

$$R_{net}^{SRH} = \frac{np - n_i^2}{\tau_p(n+n_1)+\tau_n(p+p_1)} \qquad (7)$$

in which n and p are the electron and hole concentrations, n_i is the intrinsic carrier concentration, τ_n and τ_p are the electron and hole lifetimes. The values of n_1 and p_1 correspond to electron and hole concentrations calculated when the quasi-Fermi energy is equal to the trap energy E_T.For these simulations we considered that the electron and hole lifetimes depend on temperature according to the formula presented by Schenk in Ref. 26, namely

$$\tau_{n|p}(T) = \tau_{n|p}(300)\left[\frac{300}{T}\right]^{3/2} \qquad (8)$$

where $\tau_{n|p}(300)$ is the SRH recombination lifetime at room temperature. The overall SRH lifetime (τ_{SRH}) was calculated according to the simpler formulation

$$R_{SRH} = An = \frac{1}{\tau_{SRH}} n \quad (9)$$

Parameters common to all simulations are listed in Table II.

TABLE II. Parameters common to all simulations.

	InGaN	GaN	AlGaN	Units
C_n	6.7	200	200	10^{-32} cm^6s^{-1}
C_p	6.7	200	200	10^{-32} cm^6s^{-1}
$\mu_n(300K)$	300	300	300	$cm^2V^{-1}s^{-1}$
$\mu_p(300K)$	10	10	10	$cm^2V^{-1}s^{-1}$
α_n	1.5	1.5	1.5	-
α_p	2.0	2.0	2.0	-
B	–	2.0	2.0	10^{-11} cm^3s^{-1}
m_e	0.188	0.2	0.2	-
m_h	1.67	1.5	1.09	-

The results of the simulations are reported in Fig. 3: as can be noticed in Fig. 3 (a), by numerical calculations the dependence of the τ_{SRH} on temperature can be accurately reproduced by the simulations. Fig. 3 (b) reports the experimental thermal droop, compared with the simulated data, obtained by taking into account the variation of τ_{SRH} with temperature reported in Fig. 3 (a). The results of this analysis demonstrate a poor correspondence between the experimental data and the simulated behavior, and indicate that thermal droop cannot be simply explained by considering that high temperatures induce an increase in non-radiative SRH recombination. An additional mechanism must be therefore taken into account.

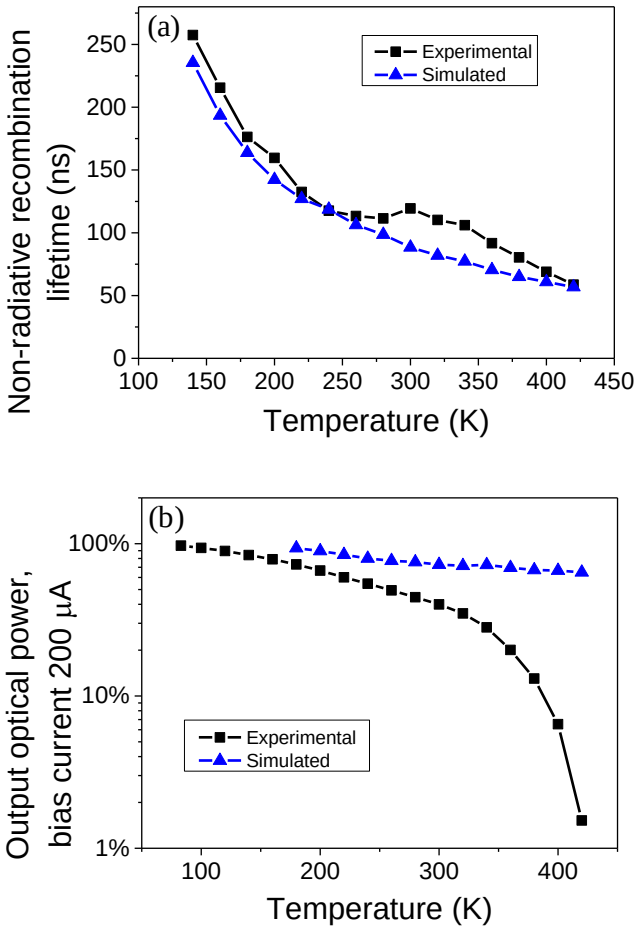

Fig. 3 : Comparison between the experimental amount and a simulation of the SRH recombination contribution for (a) SRH lifetime and (b) thermal droop. SRH recombination lifetime was evaluated by means of differential carrier lifetime measurements

B. Stress experiments

A second argument to demonstrate that thermal droop does not only depend on the increase in SRH recombination at high temperatures was obtained through the execution of degradation tests.

The idea is to forcibly induce a change in defect concentration (by applying a high constant current), and to track the effects it has on the device. The LED was submitted to 100 mA constant bias at 75 °C, and at each stress step we monitored the current-voltage characteristic, the output optical power and the differential carrier lifetime. Moreover, the photoluminescence and corresponding photocurrent were obtained through a custom setup employing a 405 nm laser diode and an optical system able to reach excitation levels up to 50 W/mm^2. The results are summarized in Fig. 4.

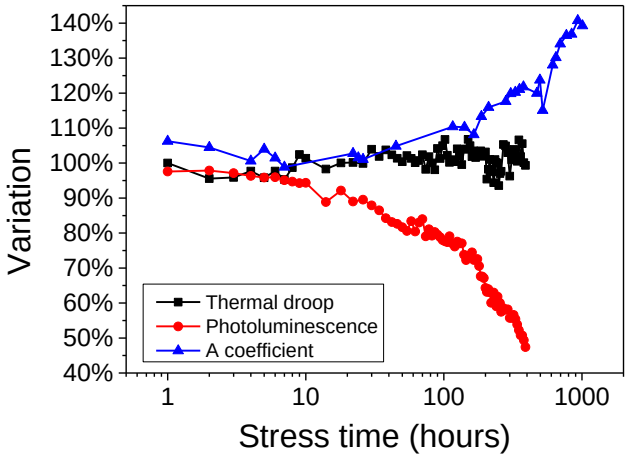

Fig. 4 : Variation of thermal droop, photoluminescence level and SRH A coefficient over stress at 100 mA, 75 °C.

During stress, we detected a clear increase of the SRH A coefficient, which is related to the non-radiative recombination through deep levels, suggesting an increase of the defect concentration inside the quantum well. The same conclusion is supported also by the strong decrease of the photoluminescence level: since no increase of the photocurrent was detected, the photogenerated electron-hole pairs are lost due to the recombination through the higher number of defective states. Even though these two quantities indicate a higher defect density inside the quantum well, no significant variation of the thermal droop was induced by the stress. This result is a further evidence of the fact that thermal droop does not solely depend on the amount of SRH recombination within the quantum well.

C. Impact of electron blocking layer

Another indication of the fact that SRH recombination is not the main cause of thermal droop comes from the fact that an improvement of the electron blocking layer (EBL) can result in a significant reduction of the thermal droop[2,4,10]. This suggests that another possible mechanism for explaining thermal droop is the escape of carriers from the quantum wells.[4,10,15,27]

IV. ESCAPE MECHANISMS

In order to provide a better understanding of the processes responsible for thermal droop, we evaluated the impact of carrier escape mechanisms on the optical efficiency of the devices.

A critical parameter is the distance between the lower border of the conduction band and the lowest allowed energetic level inside the quantum well $E_C - E_0$; this was calculated by starting from the

unstrained energy gap, introducing strain[28], evaluating the band profile and solving the Schrödinger problem for the conduction band in flat-band approximation.

A. Thermionic escape

The first escape mechanism we evaluated is the simple thermionic escape (Fig. 5 (a)): here the electrons inside the well are able to overcome the barrier energy $V_B = E_C - E_1$ thanks to the thermal energy, and then they can escape into the barrier layer. The band diagrams reported in this paper are simple sketches intended as visual aid for the reader, for an easier understanding of the different models, they are not accurate representations of the device. The closed-form equation describing this mechanism was derived by Schneider *et al.*,[29] and was used for studying the carrier escape from InGaN quantum wells of solar cells (e.g. by Lang *et al.*).[30] The electron flow balance (inside and outside the well) is evaluated from the energy distribution of the carrier density inside the well, by obtaining the relation

$$\tau_{therm_esc} = \sqrt{\frac{2\pi m^* L_w^2}{k_B T}} \exp\left(\frac{E_C - E_1}{k_B T}\right) \qquad (10)$$

where τ_{therm_esc} is the average time required for the escape of one electron, m^* the electron effective mass inside the well and L_W the well thickness. The results are reported in Fig. 5 (b), and show that the dependence on the temperature of the experimental data strongly differs from the theoretical relation of pure thermal escape calculated based on (10). Moreover, the simple thermal escape model is not able to explain the fact that thermal droop depends on defect density, as highlighted in Fig. 2. Therefore, a pure thermionic escape process from the quantum well is not a likely candidate as the cause for the thermal droop, at least in the blue spectral range considered within this paper.

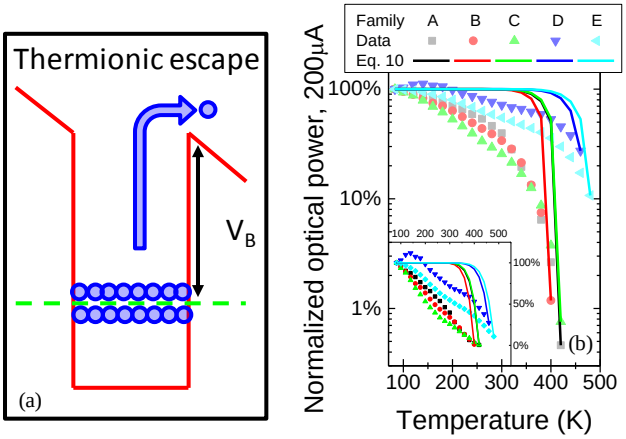

Fig. 5 : (a) Sketch of the pure thermionic escape process and (b) fitting of the experimental data.

B. Phonon-assisted tunneling

A possible reason for this may be the fact that the pure thermionic model in Fig. 5 (a) does not consider any defect- and phonon-related escape process, such as tunneling. We therefore considered a more accurate model to simulate carrier escape, namely phonon-assisted tunneling (PAT). This process, described in Figure 6 (a), consists of the tunneling of the electron from the QW, enhanced by the coupling of the electrons with the phonons and by the electric field. The widely diffused equation derived by Pons *et al.*[31] – which was successfully used by Kim *et al.* in the analysis of the reverse-bias current-voltage characteristics of InGaN-based LEDs[32] – was found to provide a reasonable fit of our experimental data (see Figure 6 (b)). The emission rate from the quantum well can be briefly expressed as

$$e_F(T) \propto \left(1 - e^{-\hbar\omega/k_B T}\right) \sum_{n=0}^{\infty} e^{-n\hbar\omega/k_B T} \qquad (11)$$

where e_F is the field-enhanced emission rate and $\hbar\omega$ the energy of the phonon which has the strongest coupling with the electrons (the complete formulation we used is lengthy and can be found in section IV.D or in the paper by Pons[31]). Fig. 6 (b) shows some agreement between the data and the model; however, the PAT model in (11) does not explain the relation between defect density and the thermal droop.

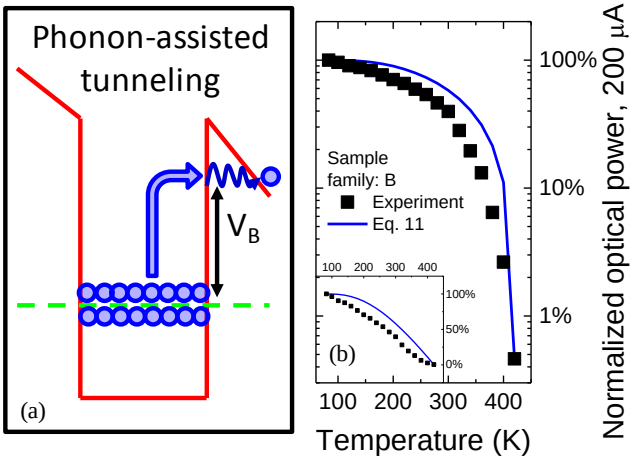

Fig. 6 : (a) Sketch of the phonon-assisted tunneling escape process and (b) fitting of the experimental data.

C. Thermionic trap-assisted tunneling

A more complex model, that allows to consider the role played by deep levels and also the effect of thermal processes, is the thermionic trap-assisted tunneling (TTAT) in its widespread formulation developed by Sathaiya *et al.* for Schottky diodes described in Fig. 7 (a).[33,34] The first part of the mechanism (A) is a field- and temperature-assisted emission from the quantum well to an intermediate deep level, while the second part (B) is a pure tunneling process from the deep level to the edge of the conduction band, described in this case by using the Wentzel-Kramers-Brillouin (WKB) approximation.

To use this model, it is necessary to collect information on the presence/properties of the deep levels within the active region of the devices. For this reason, we carried out C-DLTS measurements on all sample families, by using a filling voltage of 1 V and a measure voltage of -2 V in the temperature range from 83 K to 475 K. We detected three trap states: one hole trap H1 at $E_{H1} \sim E_V + 1$ eV and two electron traps E1 at $E_{E1} \sim E_C - 0.8$ eV and E2 at $E_{E2} \sim E_C - 0.33$ eV. Hole traps in gallium nitride described by similar signatures have already been reported in the literature,[35–37] and they may be related to gallium vacancies.[38] Concerning the electron traps, the first one has been detected several times in n-GaN,[39–41] and has been ascribed to native point defects introduced during GaN growth.[42] The E2 level is similar to the one detected by other groups in GaN layers,[36,43,44] possibly related to N vacancy complexes.[45] Since it is an intrinsic defect in gallium nitride and is placed between the bottom of the conduction band and the lowest allowed energetic level inside the quantum well, it is a likely candidate for the TTAT mechanism.

This approach is also not able to completely reproduce the experimental behavior (see Fig. 7 (b)), due to the very high barrier for the pure tunneling part (B) of the process. The latter causes a very slow emission from the deep level that dominates in the overall balance and produces an almost temperature-independent mechanism, since the tunneling is not thermally-assisted in this formulation.

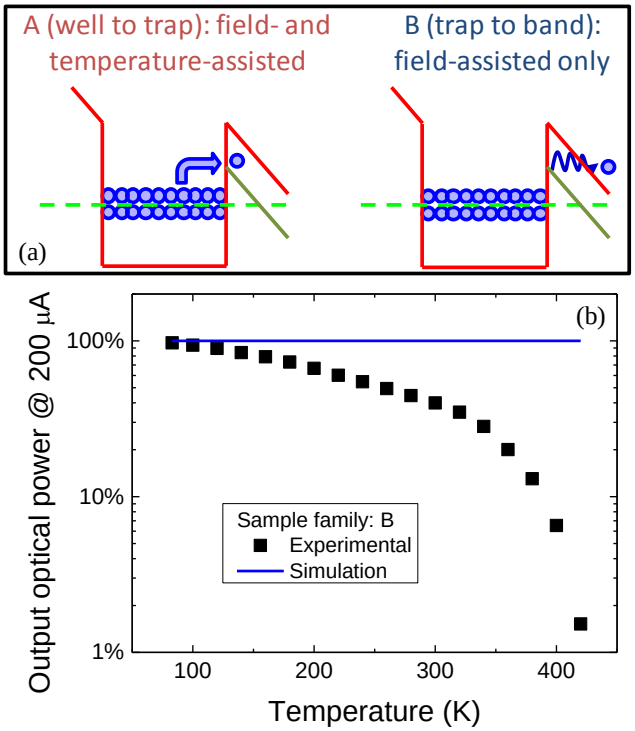

Fig. 7 : (a) Sketch of the thermionic trap-assisted tunneling escape process and (b) fitting of the experimental data.

D. Extended thermionic trap-assisted tunneling

To overcome the limitations of the models described above, we developed a new model, called extended thermionic trap-assisted tunneling (ETTAT), in order to take into account the role of the temperature also in the second part of the emission process. A sketch of the suggested mechanism is reported in Fig. 8. Even if, at first sight, the escape process may seem similar to the TTAT of Fig. 7 (a), it is important to point out that the equation set describing process "P1" and "P2" vastly differ from the equations of "A" and "B" derived by Sathaiya *et al.*, since we employ for each part Pons's phonon assisted tunneling. Moreover, process "P2" takes into account the effect of temperature. A detailed description of the model is given in the following section.

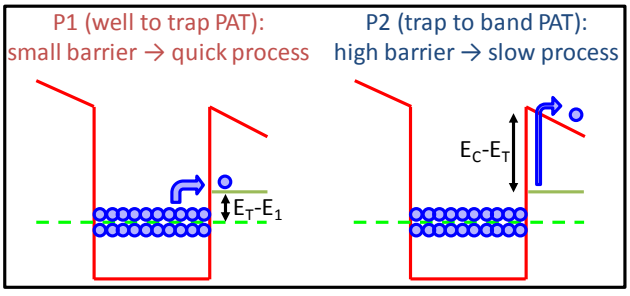

Fig. 8 : Sketch of the proposed extended thermionic trap-assisted tunneling escape process.

1. Model formalism

The carrier escape processes consists in two steps with the same analytical description, from the well to the trap (P1), and from the trap to the conduction band (P2, see Fig. 8). Each step is defined by an extension of the phonon-assisted tunneling. The equation (11) is the field-assisted part of the process, but we have to add the component of the thermal emission at zero bias, as was stated but not calculated in the original derivation by Pons *et al.* (see equation (18) in Ref. 31). Each step then assumes the complete description

$$e(T) = e_T(T) + k \cdot e_F(T) \tag{12}$$

where e is the total emission rate, e_T, e_F are the zero-bias thermal emission rate and the field-enhanced emission rate as per equation (11), respectively, and k is a fitting parameter.

Concerning the pure thermal emission, as discussed in equation (10), we can set

$$e_T(T) = \frac{1}{\tau_{therm_esc}} = \sqrt{\frac{k_B T}{2\pi m^* L_w^2}} \exp\left(-\frac{\Delta E}{k_B T}\right) \tag{13}$$

substituting ΔE with the relevant distances, E_T - E_1 and E_C - E_T, respectively, for the well to trap (P1) and trap to band (P2) step. All these energy values are not fitting parameters but actual data taken from the DLTS analysis and from the simulations, so they confer consistency to the results of the theoretical analysis.

The complete formula for the field-assisted part briefly reported in section IV.B (see equation (11)), as summarized in equation (B.2) in Pons' paper, is

$$e_F = (1 - e^{-\hbar\omega/k_B T}) \sum_{n=0}^{\infty} \sum_{p} e^{-n\hbar\omega/k_B T} \Gamma(\Delta_p) J_p^2 \left[2\sqrt{S\left(n + \frac{1}{2}\right)} \right] \tag{14}$$

where n is the number of phonons, p the order of the phonon energy level, Δ_p the energy difference between the conduction band edge and the phonon energy level of order p and S the Huang-Rhys factor. Moreover, other elements in this equation that can be expanded are the Bessel function of the first kind J_p

$$J_p(x) = \frac{1}{2\pi} \int_{-\pi}^{\pi} e^{i(p\tau - x\sin\tau)} d\tau \tag{15}$$

and Korol's formula for the ionization rate of an electron trapped in a delta function potential well (which most closely models the behavior of a deep level) $\Gamma(\Delta)$

$$\Gamma(\Delta) = \gamma \frac{\Delta}{qK} e^{-K} \tag{16}$$

where

$$\gamma = \frac{8q}{3\hbar} \tag{17}$$

is Pons' preexponential factor (q is the electronic charge) and

$$K = \frac{4}{3}\frac{2m^*}{\hbar F}\Delta^{3/2} \tag{18}$$

the WKB attenuation of the wave function across the potential barrier caused by an electric field F. By using (13) and (14) in (12), we obtain the complete equation for the ETTAT emission rate

$$e(T) = \sqrt{\frac{k_B T}{2\pi m^* L_w^2}} \exp\left(-\frac{\Delta E}{k_B T}\right) + k \cdot (1 - e^{-\hbar\omega/k_B T}) \sum_{n=0}^{\infty} \sum_{p} e^{-n\hbar\omega/k_B T} \Gamma(\Delta_p) J_p^2 \left[2\sqrt{S\left(n+\frac{1}{2}\right)}\right] \tag{19}$$

The model needs only two fitting parameters in order to produce meaningful results. The first one is the value of the electric field at the border of the quantum well, which can be estimated through simulations or experimental analyses. The second one is a scaling constant in the sum of equation (12), due to the need to obtain comparable contributions from different equations containing parameters theoretically known or experimentally extracted with a limited degree of precision and accuracy. Even though the ETTAT was used in this paper in order to explain the thermal droop of a InGaN-based LED, this formalism could be applied to any kind of detrapping process. If the thermal emission is from a deep level and not from a quantum well, at a first glance the value of the quantum well thickness L_W is missing and should be substituted with the thickness of the equivalent potential well induced by the defect, which is not easy to obtain. At a closer analysis of equation (19), we can see that L_W is a multiplicative term for the thermal emission at zero bias component, and since the model employs the multiplicative fitting parameter k for the field assisted part, any dummy value can be used for L_W without compromising the descriptive capability of the ETTAT model.

2. Calculation of relevant parameters

The derived ETTAT formulation (see equation (19)) contains several physical constants, but also some device- and material-related parameters that need to be calculated.

The Huang-Rhys factor S and the energy of the phonon with the strongest coupling to the electrons $\hbar\omega$ can be evaluated from electroluminescence (EL) spectral measurements at low temperature.[46] Even if these values are typically obtained from photoluminescence (PL) tests, the figures reported in the literature and experimentally derived in this paper are consistent with PL reports[47–51], as are the ones in cathodoluminescence (CL) studies.[52] The spectra present one or more secondary peaks, called phonon replicas, caused by the interaction between the electron-hole pair and one or more phonons. The energy separation between neighboring peaks is the energy of the phonon, typically a longitudinal-optical (LO)

phonon, while the Huang-Rhys factor can be calculated from the peak amplitudes according to the equation

$$\frac{I_{n+1}}{I_n} = \frac{S}{n+1} \tag{20}$$

where S is the Huang-Rhys factor, n is the number of phonons involved in the process (or, equivalently, the order of the replica) and I_n and I_{n+1} the intensity of the n-th and (n+1)-th replica respectively. The process, along the experimental data, is shown in Fig. 9. We obtained $\hbar\omega$ = 90 meV and S = 0.30.

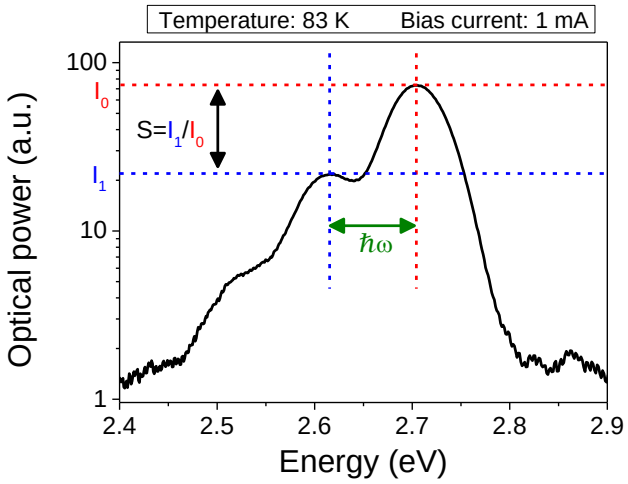

Fig. 9 : Procedure for the calculation of the phonon energy and Huang-Rhys factor from the experimental electroluminescence spectrum at low temperature.

If experimental data are not readily available, an estimate could be obtained from the literature. The LO phonon energy is calculated in the range 89-92 meV[47–57], in perfect accordance with the data presented in this paper. For the Huang-Rhys factor, reported values typically cluster in the region 0.1-0.6 [47–57], and the probable linear dependence on zero-phonon peak energy must be taken into account.[53–57]

The experimental estimation of the electron effective mass m^* is not trivial, therefore values reported in the literature for the same material system may be used. Theoretical studies compute an effective mass for GaN (m^*_{GaN}) in the range 0.179-0.26 m_0 in the direction parallel to the hexagonal axis ($m^*_{\parallel}$) and 0.18-0.28 m_0 in the perpendicular direction ($m^*_{\perp}$), where m_0 is the electron mass.[58–61] Early experimental studies suggest a value of 0.20 m_0 from normal-incidence reflectivity[62] and of 0.22-0.23 m_0 by cyclotron resonance experiments[63–66], while more accurate estimates were obtained by Witowski *et al.* (0.222 m_0[67]) and by using infrared absorption spectroscopy (0.236 m_0[68]). AlGaN/GaN heterostructure were used in order to evaluate the effective mass by Shubnikov – de Haas oscillations in the two-dimensional electron gas[69–73], obtaining values in the large interval from 0.18 m_0 to 0.228 m_0, probably due to the effect of

different magnetic fields[73] or to the different electron wave-function penetration into the barrier layer.[74] Perlin *et al.*[75] calculated 0.22 m_0 by infrared reflectivity, and derived almost no difference between the parallel and perpendicular component of the effective mass, a very important result partly supported by the data obtained by Kasic *et al.*[76] through infrared spectroscopic ellipsometry, yielding similar values for $m_{\parallel}^{*}$ (0.228 m_0) and $m_{\perp}^{*}$ (0.237 m_0).

Concerning indium nitride (m^*_{InN}), theoretical studies yield values in the range 0.058-0.07 m_0 in the direction parallel to the hexagonal axis and 0.061-0.073 m_0 in the perpendicular direction.[59–61] Experimental studies report values of 0.12 m_0 by reflection spectra[77], 0.14 m_0 by infrared spectroscopic ellipsometry[78] and a larger 0.24 m_0.[79] More recent papers find a strong reduction of the effective mass, 0.07 m_0 and 0.05 m_0 by infrared reflection experiments[80,81], while by infrared magneto-optic generalized ellipsometry values in the range 0.039-0.090 m_0 for $m_{\parallel}^{*}$ and 0.047-0.090 m_0 for $m_{\perp}^{*}$ were obtained.[82]

Taken into account the theoretical and experimental reports, we suggest m^*_{GaN} = 0.20 m_0 and m^*_{InN} = 0.07 m_0, in accordance with Ref. 83. The electron effective mass in InGaN can then be estimated through a linear interpolation[84–86] (method supported also by some tight-binding calculations[87]) as

$$m^*_{In_xGa_{1-x}N} = m^*_{GaN} + x(m^*_{InN} - m^*_{GaN}) \qquad (21)$$

Even though there are papers describing the dependence of m^* on the free electron concentration in InN[80–82], at the best of our knowledge the same issue has not been reported yet for GaN or InGaN, therefore we may assume the values obtained through equation (21) to be reliable.

3. Thermal droop modeling

In our specific case, the difference between the energetic barriers of the two steps P1 and P2 is so high (0.2 eV to 0.3 eV) that the deep level is easily filled by the very fast P1 process. Therefore, the escape rate from the quantum well is limited by the time required to empty the defective state, which acts as an intermediate reservoir of electrons. The number of escaped electrons is proportional to the density of defects,[88–90] giving an increased carrier loss (and then a more intense thermal droop) in the devices with higher defect density, consistent with the experimental findings (see Fig. 1). It is useful to point out that this loss mechanism depends on the first power of the carrier density, therefore it could cause a variation of the A SRH coefficient which may be incorrectly ascribed to an increase of the non-radiative recombination.

Fig. 10 (b) shows that the developed ETTAT model provides a very good agreement with the experimental data, while Fig. 10 (c) shows the breakdown of the curve into the two components: the zero-bias thermionic and the field-assisted part. Fig. 10 (a) reports the same sketch of Fig. 8 for reference. The value of k in (19) should theoretically equal unity, and in our case the fitted value is 0.33, a good agreement if the possible variations caused by the estimate of the effective mass from the literature, by the calculation of the Huang-Rhys factor and of the phonon energy and by the emission energy accuracy of

the DLTS system are taken into account. This defect-enhanced escape mechanism may also play a role in explaining the unexpected carrier transport during resonant optical excitation measurements.[91]

Even though the role of the pure thermionic escape in Fig. 10 (c) may seem small, its contribution should not be overlooked. The presence of the thermionic escape in the model is needed as per Eq. 12, and it causes nearly 16% of the total thermal droop. Pure thermionic escape would have an even higher impact in case of higher measurement temperature or shallower $E_C - E_T$ barrier.

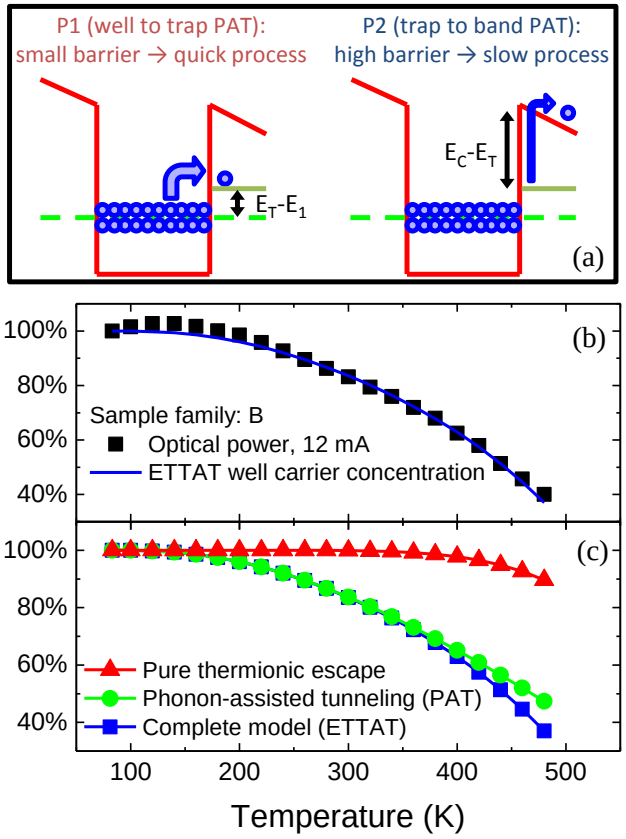

Fig. 10 : (a) Sketch of the proposed escape model (for reference), (b) agreement between the experimental data and the developed model and (c) breakdown of the overall curve into the two components.

The suggested ETTAT formulation describes a rate-limited process, whose limiting quantity is the defect density of the intermediate deep level. In a simple electrical model, it can be regarded to as a leakage path with low maximum current (related to the maximum number of escape events through the fixed number of defects) shunting the quantum well. Therefore, the amount of thermal droop should be higher at low bias current levels, where the number of escaped electrons is a large portion of the total injected current, and decrease with increasing bias, due to the lower escaped – injected electrons ratio. As reported in Fig. 11, this behavior of the model is consistent with the experimental data. Since the escape

mechanism has a maximum rate, a possible contribution of SRH non-radiative recombination to the thermal droop in every possible defect position and concentration, bias and device structure combination can not be excluded. Moreover, the carrier escape model presented in this paper requires a deep level present at an energy level between the lower edge of the conduction band and the lowest allowed state inside the quantum well in order to contribute to the overall thermal droop.

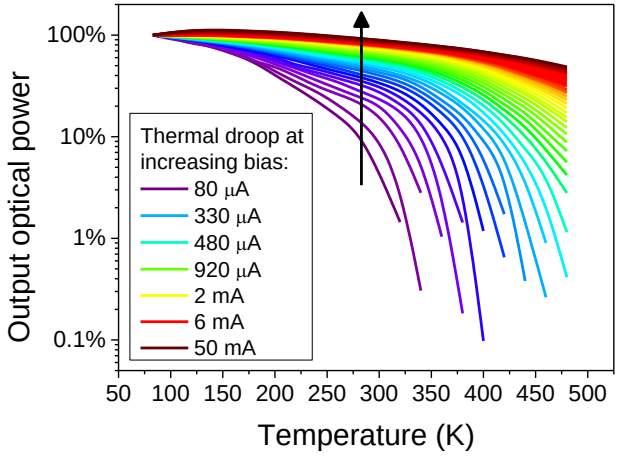

Fig. 11 : Dependence of the thermal droop on bias current.

In summary, within this work we demonstrated the correlation between the drop of the optical power with increasing temperature in InGaN-based SQW LEDs and the concentration of defects. In order to explain this finding, we have reviewed some mechanisms that are believed to be related to the efficiency of the device, such as the Shockley-Read-Hall recombination, the thermionic escape of carriers from the quantum well and other field-assisted escape mechanisms, namely the phonon-assisted tunneling and the thermionic trap-assisted tunneling. Each of these processes has some specific properties that - for the samples under investigation - make it unable to fully explain the whole set of experimental data, so we developed a new model called extended thermionic trap-assisted tunneling. It consists of a two-step zero bias extended phonon-assisted tunneling from the quantum well to the trap, which acts as an intermediate reservoir of electrons, and from the quantum well to the border of the conduction band. By using parameters extracted from simulation of the energetic structure of the quantum wells and from C-DLTS characterization of the deep levels, the obtained closed-form equation was able to accurately fit the data on the thermal droop of five different families of GaN-on-Si LEDs.

[1] Y.C. Shen, G.O. Mueller, S. Watanabe, N.F. Gardner, A. Munkholm, and M.R. Krames, Appl. Phys. Lett. **91**, 141101 (2007).

[2] J. Iveland, L. Martinelli, J. Peretti, J.S. Speck, and C. Weisbuch, Phys. Rev. Lett. **110**, 177406 (2013).

[3] M. Binder, A. Nirschl, R. Zeisel, T. Hager, H.J. Lugauer, M. Sabathil, D. Bougeard, J. Wagner, and B. Galler, Appl. Phys. Lett. **103**, 071108 (2013).

[4] C. Huh and S.-J. Park, Electrochem. Solid-State Lett. **7**, G266 (2004).

[5] H.K. Lee, J.S. Yu, and Y.T. Lee, Phys. Status Solidi a **207**, 1497 (2010).

[6] D.S. Meyaard, Q. Shan, J. Cho, E.F. Schubert, S.H. Han, M.H. Kim, C. Sone, S.J. Oh, and J.K. Kim, Appl. Phys. Lett. **100**, 081106 (2012).

[7] D.L. Becerra, Y. Zhao, S.H. Oh, C.D. Pynn, K. Fujito, S.P. DenBaars, and S. Nakamura, Appl. Phys. Lett. **105**, 171106 (2014).

[8]Figures from Commercially-Available LED Datasheets: Cree XREROY, LedEngin LZ4-00B210, Lumileds LXML-PR01, Osram LD W5SM, Seoul Semiconductor D42180.

[9] C.C. Pan, T. Gilbert, N. Pfaff, S. Tanaka, Y. Zhao, D. Feezell, J.S. Speck, S. Nakamura, and S.P. DenBaars, Appl. Phys. Express **5**, 102103 (2012).

[10] K.S. Kim, J.H. Kim, S.J. Jung, Y.J. Park, and S.N. Cho, Appl. Phys. Lett. **96**, 091104 (2010).

[11] M. Meneghini, M. La Grassa, S. Vaccari, B. Galler, R. Zeisel, P. Drechsel, B. Hahn, G. Meneghesso, and E. Zanoni, Appl. Phys. Lett. **104**, 113505 (2014).

[12] B. Galler, P. Drechsel, R. Monnard, P. Rode, P. Stauss, S. Froehlich, W. Bergbauer, M. Binder, M. Sabathil, B. Hahn, and J. Wagner, Appl. Phys. Lett. **101**, 131111 (2012).

[13] D. Schiavon, M. Binder, M. Peter, B. Galler, P. Drechsel, and F. Scholz, Phys. Status Solidi B **250**, 283 (2013).

[14] A. Laubsch, M. Sabathil, J. Baur, M. Peter, and B. Hahn, IEEE Trans. Electron Devices **57**, 79 (2010).

[15] C.K. Wang, Y.Z. Chiou, and D.J. Sun, ECS J. Solid State Sci. Technol. **2**, Q104 (2013).

[16] S. Chhajed, J. Cho, E.F. Schubert, J.K. Kim, D.D. Koleske, and M.H. Crawford, Phys. Status Solidi a **208**, 947 (2011).

[17] Y. Kawakami, Y. Narukawa, K. Omae, S. Fujita, and S. Nakamura, Phys. Status Solidi a **178**, 331 (2000).

[18] S.F. Chichibu, M. Sugiyama, T. Onuma, T. Kitamura, H. Nakanishi, T. Kuroda, A. Tackeuchi, T. Sota, Y. Ishida, and H. Okumura, Appl. Phys. Lett. **79**, 4319 (2001).

[19] S. Khatsevich, D.H. Rich, X. Zhang, and P.D. Dapkus, J. Appl. Phys. **102**, 093502 (2007).

[20] E. Berkowicz, D. Gershoni, G. Bahir, E. Lakin, D. Shilo, E. Zolotoyabko, A.C. Abare, S.P. Denbaars, and L.A. Coldren, Phys. Rev. B **61**, 10994 (2000).

[21] N. Can, S. Okur, M. Monavarian, F. Zhang, V. Avrutin, H. Morkoç, A. Teke, and Ü. Özgür, Proc. SPIE **9363**, 93632U (2015).

[22] M. Calciati, M. Goano, F. Bertazzi, M. Vallone, X. Zhou, G. Ghione, M. Meneghini, G. Meneghesso, E. Zanoni, E. Bellotti, G. Verzellesi, D. Zhu, and C. Humphreys, AIP Adv. **4**, 067118 (2014).

[23] S.L. Chuang, J. Quantum Electron. **32**, 1791 (1996).

[24]*Crosslight Device Simulation Software - General Manual* (Crosslight Software, 2013).

[25] W. Shockley and W.T. Read, Phys. Rev. **87**, 835 (1952).

[26] A. Schenk, Solid. State. Electron. **35**, 1585 (1992).

[27] K.T. Lam and S.J. Chang, J. Disp. Technol. **10**, 1078 (2014).

[28] T.Y. Wang and G.B. Stringfellow, J. Appl. Phys. **67**, 344 (1990).

[29] H. Schneider and K. V. Klitzing, Phys. Rev. B **38**, 6160 (1988).

[30] J.R. Lang, N.G. Young, R.M. Farrell, Y.R. Wu, and J.S. Speck, Appl. Phys. Lett. **101**, 181105 (2012).

[31] D. Pons and S. Makram-Ebeid, J. Phys. France **40**, 1161 (1979).

[32] K.S. Kim, J.H. Kim, and S.N. Cho, IEEE Photonics Technol. Lett. **23**, 483 (2011).

[33] D.M. Sathaiya and S. Karmalkar, J. Appl. Phys. **99**, 093701 (2006).

[34] D.M. Sathaiya and S. Karmalkar, IEEE Trans. Electron Devices **55**, 557 (2008).

[35] E. Calleja, F.J. Sánchez, D. Basak, M. a. Sánchez-García, E. Muñoz, I. Izpura, F. Calle, J.M.G. Tijero, J.L. Sánchez-Rojas, B. Beaumont, P. Lorenzini, and P. Gibart, Phys. Rev. B **55**, 4689 (1997).

[36] F.D. Auret, W.E. Meyer, L. Wu, M. Hayes, M.J. Legodi, B. Beaumont, and P. Gibart, Phys. Status Solidi a **201**, 2271 (2004).

[37] A.R. Arehart, A. Sasikumar, G.D. Via, B. Winningham, B. Poling, E. Heller, and S.A. Ringel, in *International Electron Devices Meeting IEDM 2010*, San Francisco, United States, 6-8 December 2010, published by IEEE, pp. 20.1.1–20.1.4.

[38] P. Kamyczek, E. Placzek-Popko, V. Kolkovsky, S. Grzanka, and R. Czernecki, J. Appl. Phys. **111**, 113105 (2012).

[39] N.M. Shmidt, D. V Davydov, V. V Emtsev, I.L. Krestnikov, A.A. Lebedev, W. V Lundin, D.S. Poloskin, A. V Sakharov, A.S. Usikov, and A. V Osinsky, Phys. Status Solidi B **216**, 533 (1999).

[40] C.B. Soh, D.Z. Chi, A. Ramam, H.F. Lim, and S.J. Chua, Mater. Sci. Semicond. Process. **4**, 595 (2001).

[41] G.A. Umana-Membreno, G. Parish, N. Fichtenbaum, S. Keller, U.K. Mishra, and B.D. Nener, J. Electron. Mater. **37**, 569 (2008).

[42] U. Honda, Y. Yamada, Y. Tokuda, and K. Shiojima, Jap. J. Appl. Phys. **51**, 04DF04 (2012).

[43] D. Johnstone, S. Biyikli, S. Dogan, Y.T. Moon, F. Yun, and H. Morkoc, in *Proceedings of SPIE 5739, Light-Emitting Diodes: Research, Manufacturing, and Applications IX*, San Josè, United States, 22 January 2005, edited by S.A. Stockman, H.W. Yao, and E.F. Schubert, pp. 7–15.

[44] A.Y. Polyakov, N.B. Smirnov, A.V. Govorkov, A.V. Markov, Q. Sun, Y. Zhang, C.D. Yerino, T.S. Ko, I.H. Lee, and J. Han, Mater. Sci. Eng. B **166**, 220 (2010).

[45] D.C. Look, Z.Q. Fang, and B. Claflin, J. Cryst. Growth **281**, 143 (2005).

[46] G. Franssen, E. Litwin-Staszewska, R. Piotrzkowski, T. Suski, and P. Perlin, J. Appl. Phys. **94**, 6122 (2003).

[47] V. Kümmler, G. Brüderl, S. Bader, S. Miller, A. Weimar, A. Lell, V. Härle, U.T. Schwarz, N. Gmeinwieser, and W. Wegscheider, Phys. Status Solidi a **194**, 419 (2002).

[48] P.P. Paskov, P.O. Holtz, B. Monemar, S. Kamiyama, M. Iwaya, H. Amano, and I. Akasaki, Phys. Status Solidi B **234**, 755 (2002).

[49] S.M. Olaizola, W.H. Fan, D.J. Mowbray, M.S. Skolnick, P.J. Parbrook, and A.M. Fox, Superlattices Microstruct. **41**, 419 (2007).

[50] X.-L. Hu, J.-Y. Zhang, J.-Z. Shang, W.-J. Liu, and B.-P. Zhang, Chinese Phys. B **19**, 117801 (2010).

[51] P. Renwick, H. Tang, J. Bai, and T. Wang, Appl. Phys. Lett. **100**, 182105 (2012).

[52] Y. Estrin, D.H. Rich, S. Keller, and S.P. DenBaars, J. Phys. Condens. Matter **27**, 265802 (2015).

[53] X.B. Zhang, T. Taliercio, S. Kolliakos, and P. Lefebvre, J. Phys. Condens. Matter **13**, 7053 (2001).

[54] S. Kalliakos, P. Lefebvre, X.B. Zhang, T. Taliercio, B. Gil, N. Grandjean, B. Damilano, and J. Massies, Phys. Status Solidi a **190**, 149 (2002).

[55] R. Pecharromán-Gallego, P.R. Edwards, R.W. Martin, and I.M. Watson, Mater. Sci. Eng. B **93**, 94 (2002).

[56] D.M. Graham, A. Soltani-Vala, P. Dawson, M.J. Godfrey, T.M. Smeeton, J.S. Barnard, M.J. Kappers, C.J. Humphreys, and E.J. Thrush, J. Appl. Phys. **97**, 103508 (2005).

[57] L. Zhu and B. Liu, Solid. State. Electron. **53**, 336 (2009).

[58] M. Suzuki, T. Uenoyama, and A. Yanase, Phys. Rev. B **52**, 8132 (1995).

[59] A. Svane, N.E. Christensen, I. Gorczyca, M. van Schilfgaarde, A.N. Chantis, and T. Kotani, Phys. Rev. B **82**, 115102 (2010).

[60] L. Hsu, R.E. Jones, S.X. Li, K.M. Yu, and W. Walukiewicz, J. Appl. Phys. **102**, 073705 (2007).

[61] P. Rinke, M. Winkelnkemper, A. Qteish, D. Bimberg, J. Neugebauer, and M. Scheffler, Phys. Rev. B **77**, 075202 (2008).

[62] A.S. Barker and M. Ilegems, Phys. Rev. B **7**, 743 (1973).

[63] M. Drechsler, D.M. Hofmann, B.K. Meyer, T. Detchprohm, H. Amano, and I. Akasaki, Jap. J. Appl. Phys. **34**, L1178 (1995).

[64] Y.J. Wang, R. Kaplan, H.K. Ng, K. Doverspike, D.K. Gaskill, T. Ikedo, I. Akasaki, and H. Amono, J. Appl. Phys. **79**, 8007 (1996).

[65] W. Knap, H. Alause, J.M. Bluet, J. Camassel, J. Young, M. Asif Khan, Q. Chen, S. Huant, and M. Shur, Solid State Commun. **99**, 195 (1996).

[66] W. Knap, S. Contreras, H. Alause, C. Skierbiszewski, J. Camassel, M. Dyakonov, J.L. Robert, J. Yang, Q. Chen, M. Asif Khan, M.L. Sadowski, S. Huant, F.H. Yang, M. Goiran, J. Leotin, and M.S. Shur, Appl. Phys. Lett. **70**, 2123 (1997).

[67] A.M. Witowski, K. Pakuła, J.M. Baranowski, M.L. Sadowski, and P. Wyder, Appl. Phys. Lett. **75**, 4154 (1999).

[68] B.K. Meyer, D. Volm, a. Graber, H.C. Alt, T. Detchprohm, a. Amano, and I. Akasaki, Solid State Commun. **95**, 597 (1995).

[69] S. Elhamri, R.S. Newrock, D.B. Mast, M. Ahoujja, W.C. Mitchel, J.M. Redwing, M.A. Tischler, and J.S. Flynn, Phys. Rev. B **57**, 1374 (1998).

[70] L.W. Wong, S.J. Cai, R. Li, K. Wang, H.W. Jiang, and M. Chen, Appl. Phys. Lett. **73**, 1391 (1998).

[71] A. Saxler, P. Debray, R. Perrin, S. Elhamri, W.C. Mitchel, C.R. Elsass, I.P. Smorchkova, B. Heying, E. Haus, P. Fini, J.P. Ibbetson, S. Keller, P.M. Petroff, S.P. DenBaars, U.K. Mishra, and J.S. Speck, J. Appl. Phys. **87**, 369 (2000).

[72] T. Wang, J. Bai, S. Sakai, Y. Ohno, and H. Ohno, Appl. Phys. Lett. **76**, 2737 (2000).

[73] D.R. Hang, C.T. Liang, C.F. Huang, Y.H. Chang, Y.F. Chen, H.X. Jiang, and J.Y. Lin, Appl. Phys. Lett. **79**, 66 (2001).

[74] A.M. Kurakin, S.A. Vitusevich, S.V. Danylyuk, H. Hardtdegen, N. Klein, Z. Bougrioua, A.V. Naumov, and A.E. Belyaev, J. Appl. Phys. **105**, 073703 (2009).

[75] P. Perlin, E. Litwin-Staszewska, B. Suchanek, W. Knap, J. Camassel, T. Suski, R. Piotrzkowski, I. Grzegory, S. Porowski, E. Kaminska, and J.C. Chervin, Appl. Phys. Lett. **68**, 1114 (1996).

[76] A. Kasic, M. Schubert, S. Einfeldt, D. Hommel, and T.E. Tiwald, Phys. Rev. B **62**, 7365 (2000).

[77] T. Inushima, T. Yaguchi, A. Nagase, A. Iso, T. Shiraishi, and S. Ooya, in *Indium Phosphide and Related Materials, 1995. Conference Proceedings., Seventh International Conference on*, Hokkaido, 9-13 May 1995, published by IEEE, pp. 187–190.

[78] A. Kasic, M. Schubert, Y. Saito, Y. Nanishi, and G. Wagner, Phys. Rev. B **65**, 115206 (2002).

[79] T. Inushima, T. Shiraishi, and V.Y. Davydov, Solid State Commun. **110**, 491 (1999).

[80] J. Wu, W. Walukiewicz, W. Shan, K.M. Yu, J.W. Ager, E.E. Haller, H. Lu, and W.J. Schaff, Phys. Rev. B **66**, 201403 (2002).

[81] S.P. Fu and Y.F. Chen, Appl. Phys. Lett. **85**, 1523 (2004).

[82] T. Hofmann, T. Chavdarov, V. Darakchieva, H. Lu, W.J. Schaff, and M. Schubert, Phys. Status Solidi c **3**, 1854 (2006).

[83] I. Vurgaftman and J.R. Meyer, J. Appl. Phys. **94**, 3675 (2003).

[84] J. Piprek and S. Nakamura, Optoelectron. IEE Proc. **149**, 145 (2002).

[85] J.-Y. Chang and Y.-K. Kuo, J. Appl. Phys. **93**, 4992 (2003).

[86] W.Z. Shen, S.C. Shen, Y. Chang, W.G. Tang, J.X. Chen, and A.Z. Li, J. Appl. Phys. **80**, 5348 (1996).

[87] T. Yang, S. Nakajima, and S. Sakai, Jap. J. Appl. Phys. **34**, 5912 (1995).

[88] K.K. Leung, W.K. Fong, P.K.L. Chan, and C. Surya, J. Appl. Phys. **107**, 073103 (2010).

[89] J.C. Petrosky, J.W. McClory, T.E. Gray, and T.A. Uhlman, IEEE Trans. Nucl. Sci. **56**, 2905 (2009).

[90] W.J. Chang, M.P. Houng, and Y.H. Wang, J. Appl. Phys. **89**, 6285 (2001).

[91] M.F. Schubert, J. Xu, Q. Dai, F.W. Mont, J.K. Kim, and E.F. Schubert, Appl. Phys. Lett. **94**, 081114 (2009).

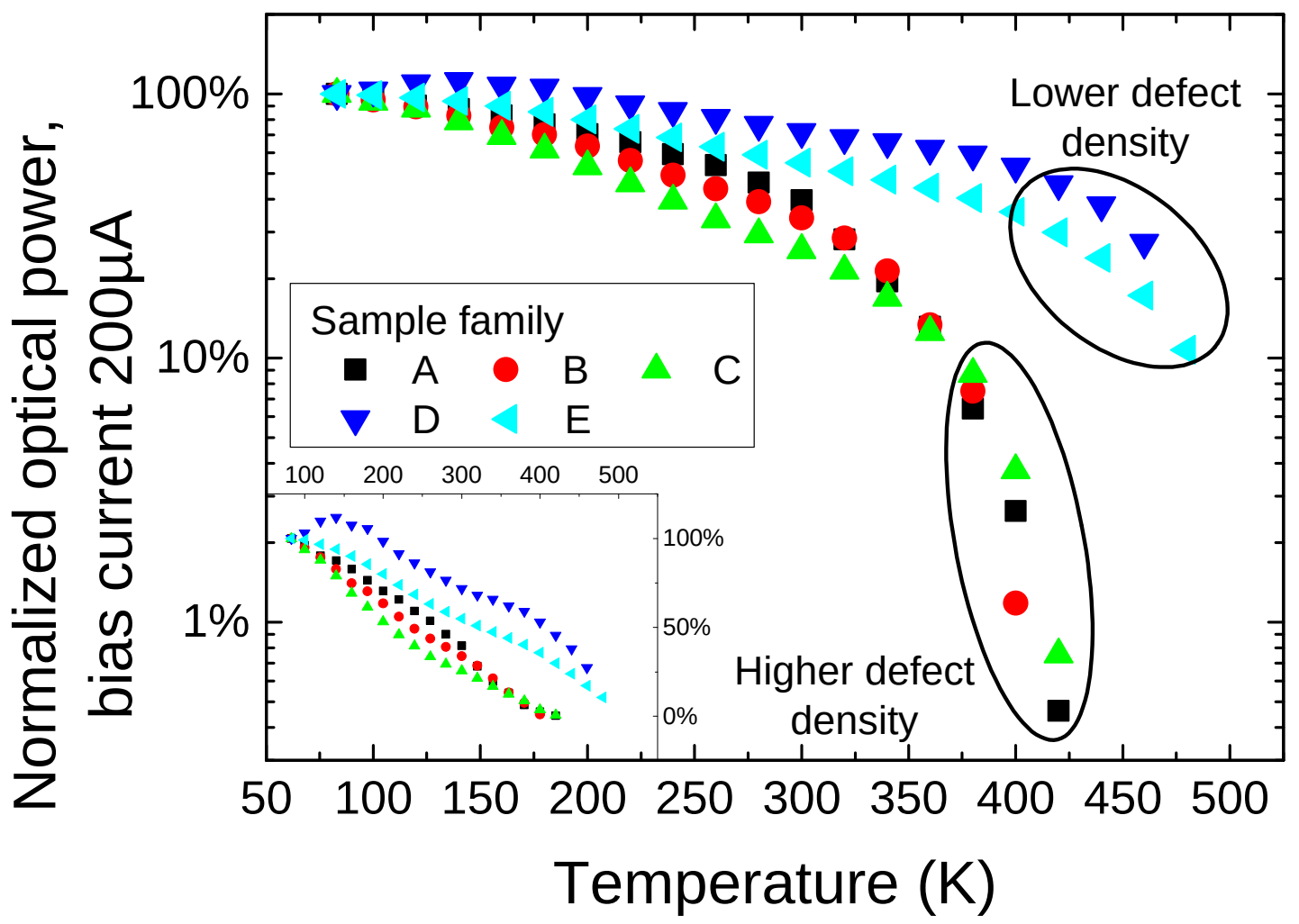
Normalized optical power, bias current 200μA
100%
10%
1%
50
100
150
200
250
300
350
400
450
500
Temperature (K)
Lower defect density
Higher defect density
Sample family
A
B
C
D
E
100
200
300
400
500
100%
50%
0%

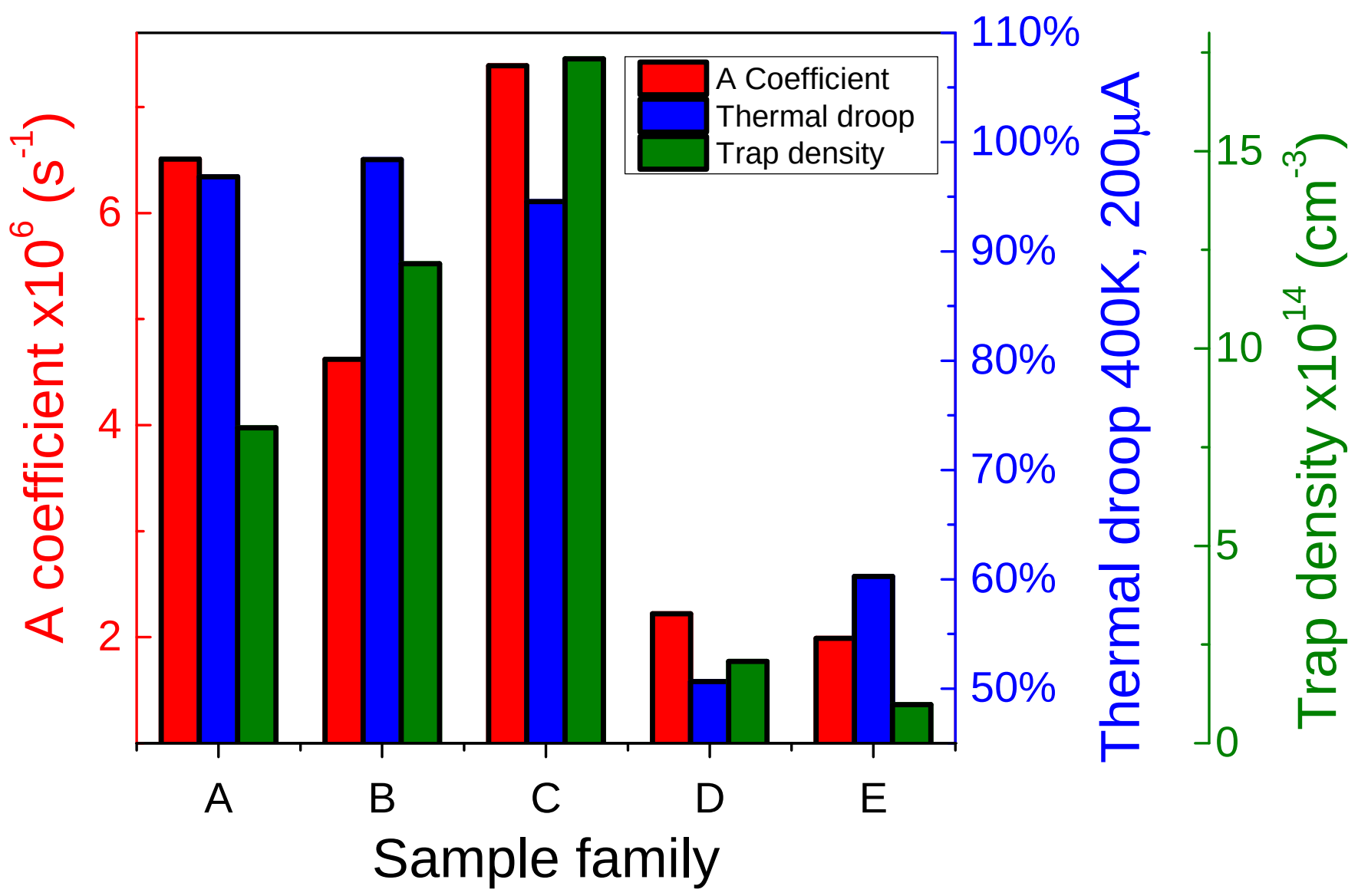
A Coefficient
Thermal droop
Trap density
A coefficient x10^6 (s^-1)
Thermal droop 400K, 200µA
Trap density x10^14 (cm^-3)
Sample family
A
B
C
D
E
2
4
6
50%
60%
70%
80%
90%
100%
110%
0
5
10
15

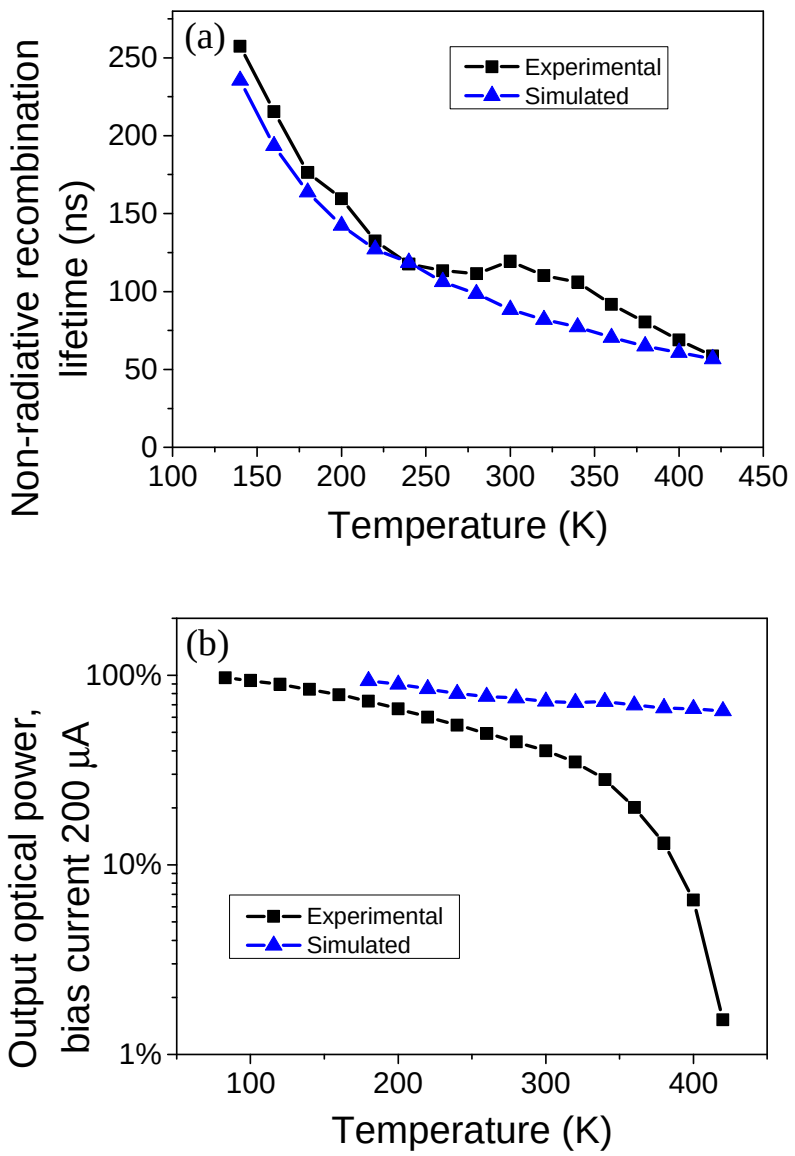
(a)
Experimental
Simulated
Non-radiative recombination lifetime (ns)
0
50
100
150
200
250
100
150
200
250
300
350
400
450
Temperature (K)
(b)
Experimental
Simulated
Output optical power, bias current 200 μA
100%
10%
1%
100
200
300
400
Temperature (K)

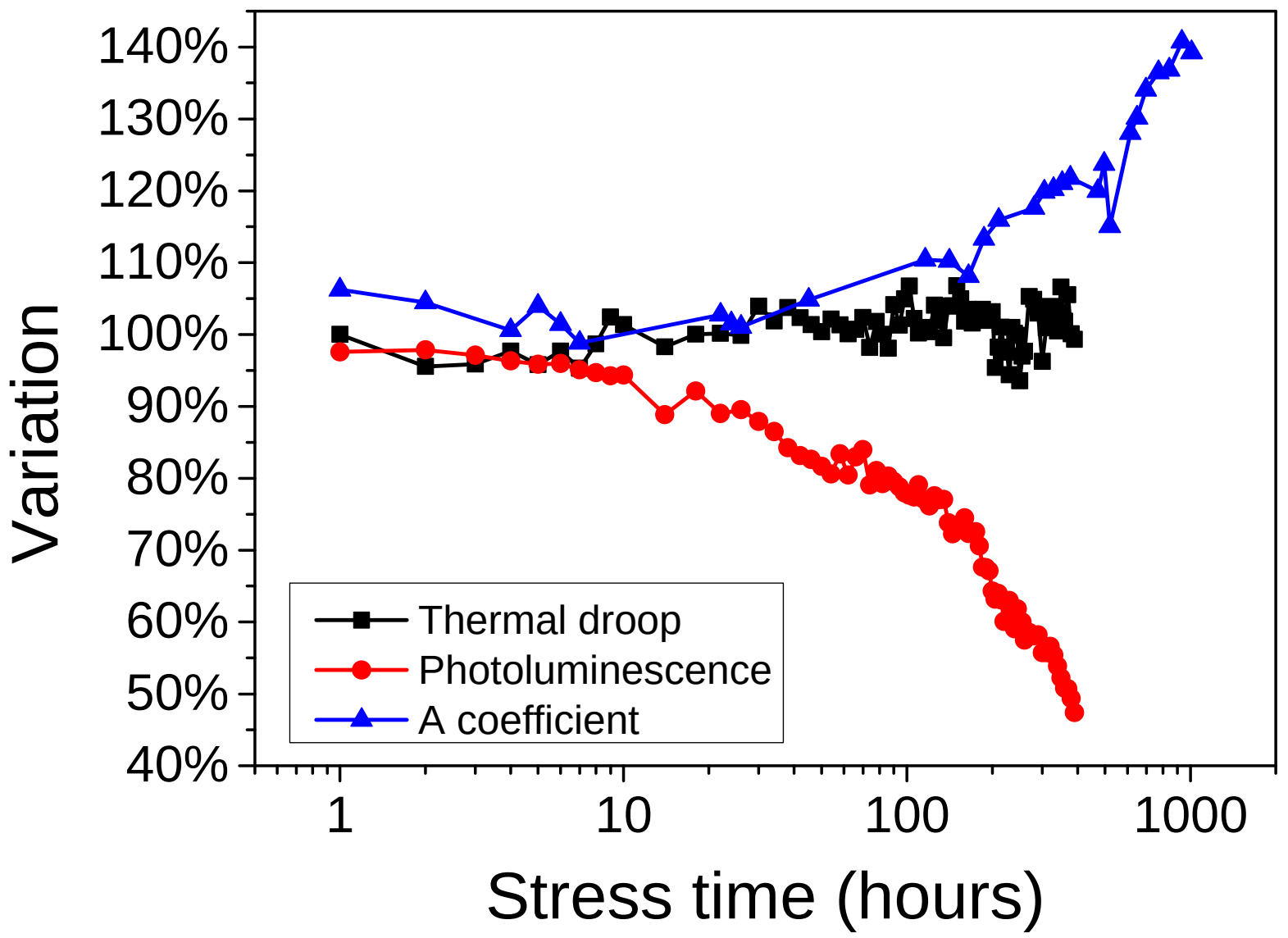
140%
130%
120%
110%
100%
90%
80%
70%
60%
50%
40%
Variation
1
10
100
1000
Stress time (hours)
Thermal droop
Photoluminescence
A coefficient

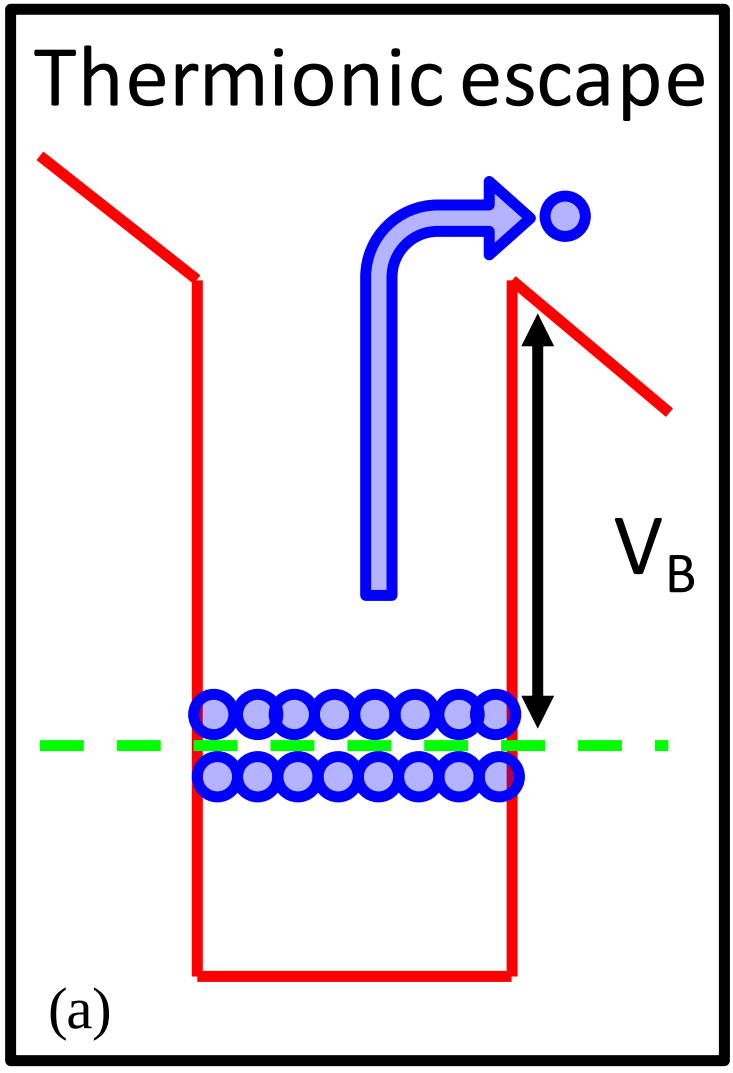
Thermionic escape
V_B
(a)

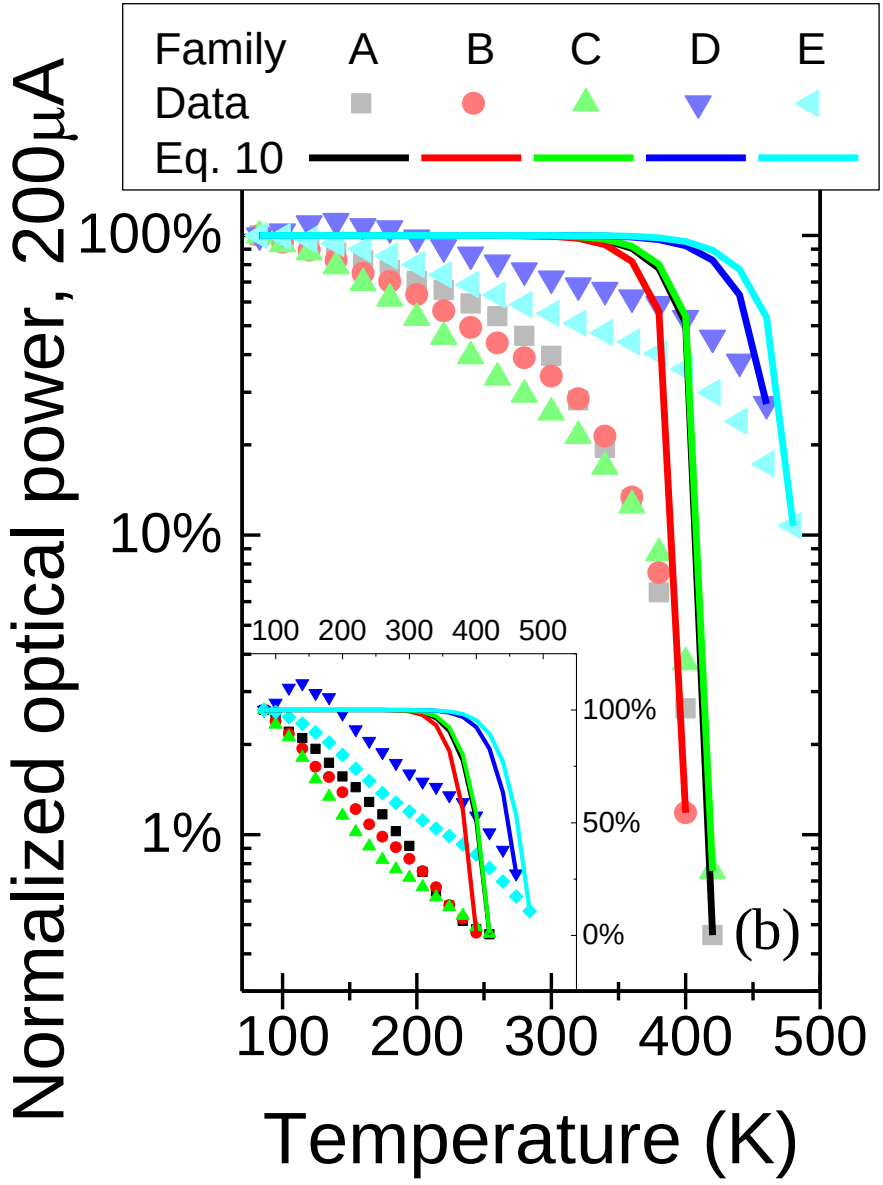
Family A B C D E
Data
Eq. 10
Normalized optical power, 200μA
100%
10%
1%
100 200 300 400 500
Temperature (K)
100 200 300 400 500
100%
50%
0%
(b)

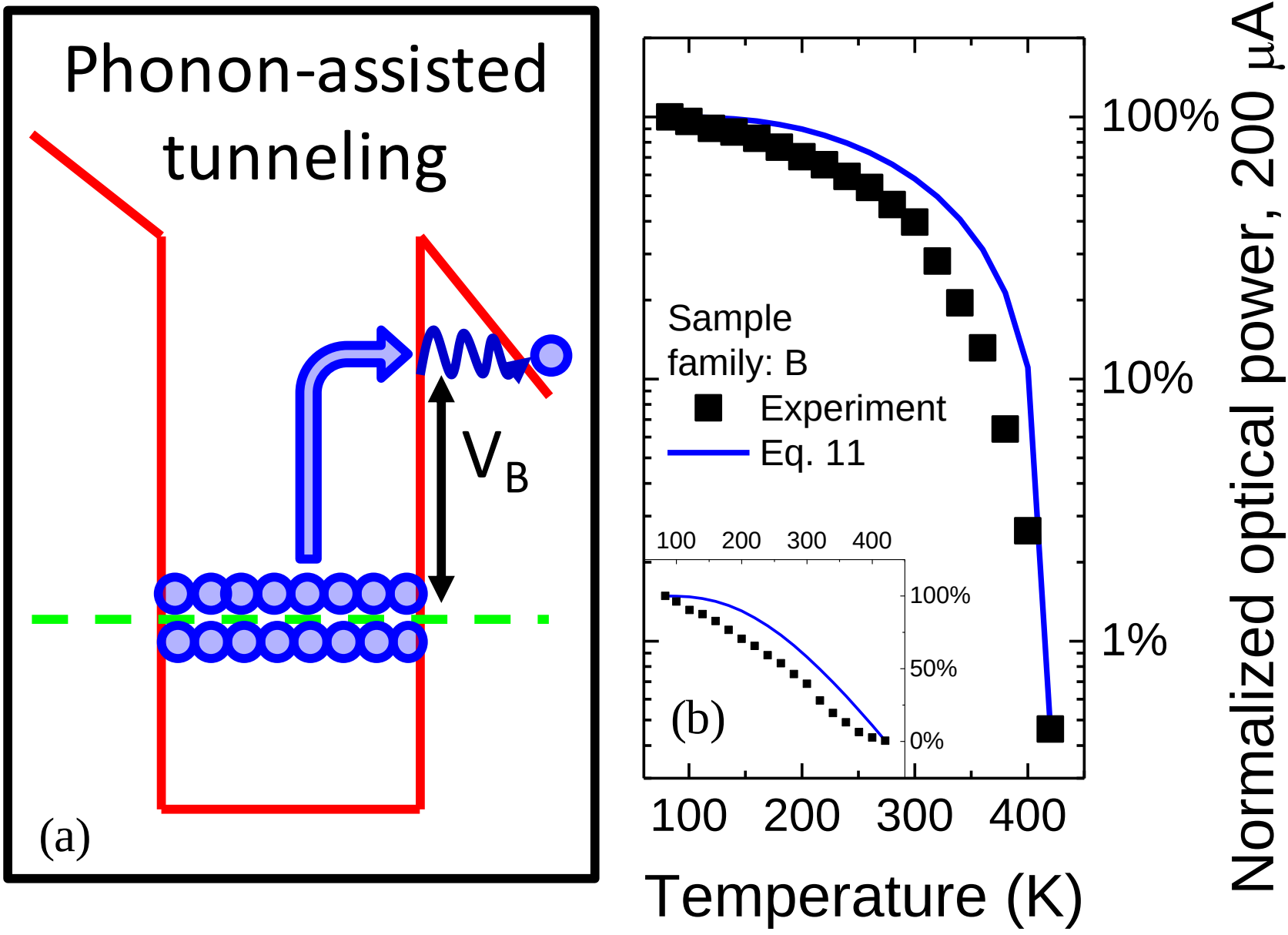
Phonon-assisted tunneling
V_B
(a)
Sample family: B
Experiment
Eq. 11
100%
10%
1%
100 200 300 400
100%
50%
0%
(b)
100 200 300 400
Temperature (K)
Normalized optical power, 200 μA

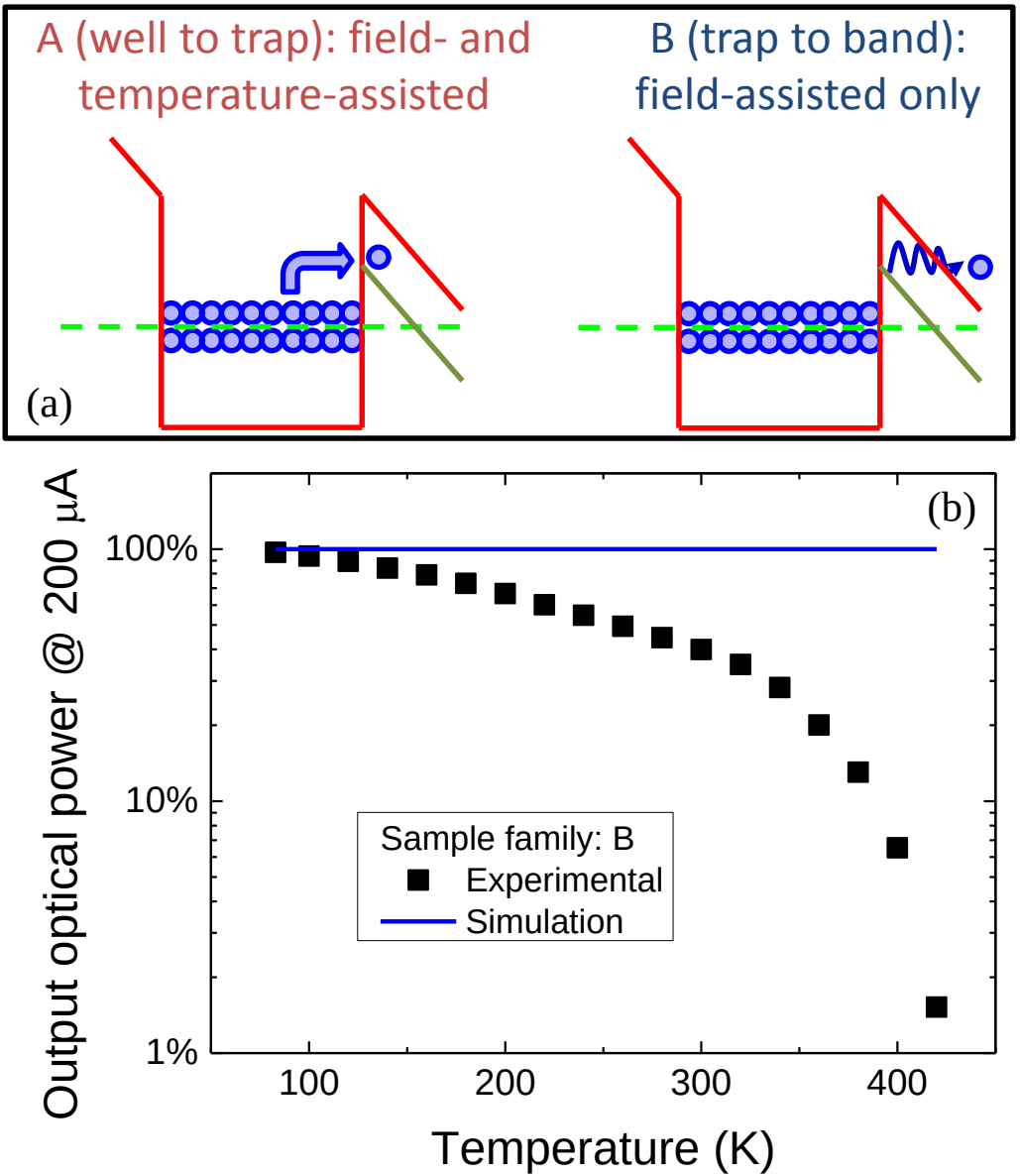
A (well to trap): field- and temperature-assisted
B (trap to band): field-assisted only
(a)
(b)
Output optical power @ 200 μA
100%
10%
1%
100
200
300
400
Temperature (K)
Sample family: B
Experimental
Simulation

P1 (well to trap PAT):
small barrier → quick process

P2 (trap to band PAT):
high barrier → slow process

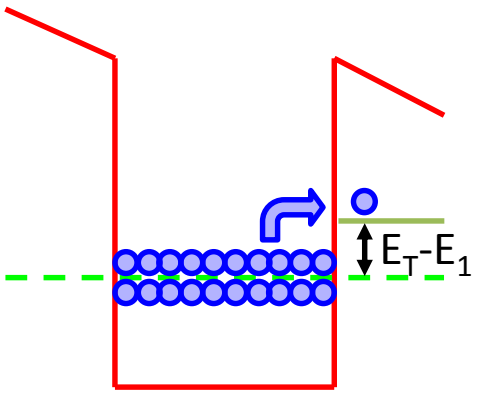

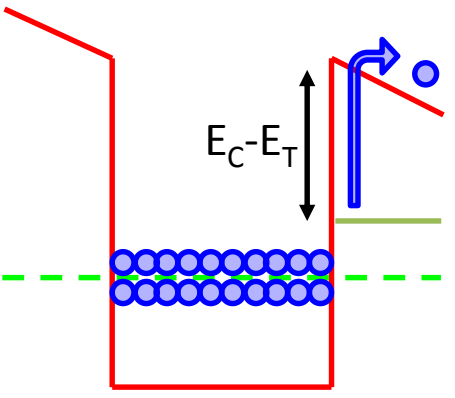

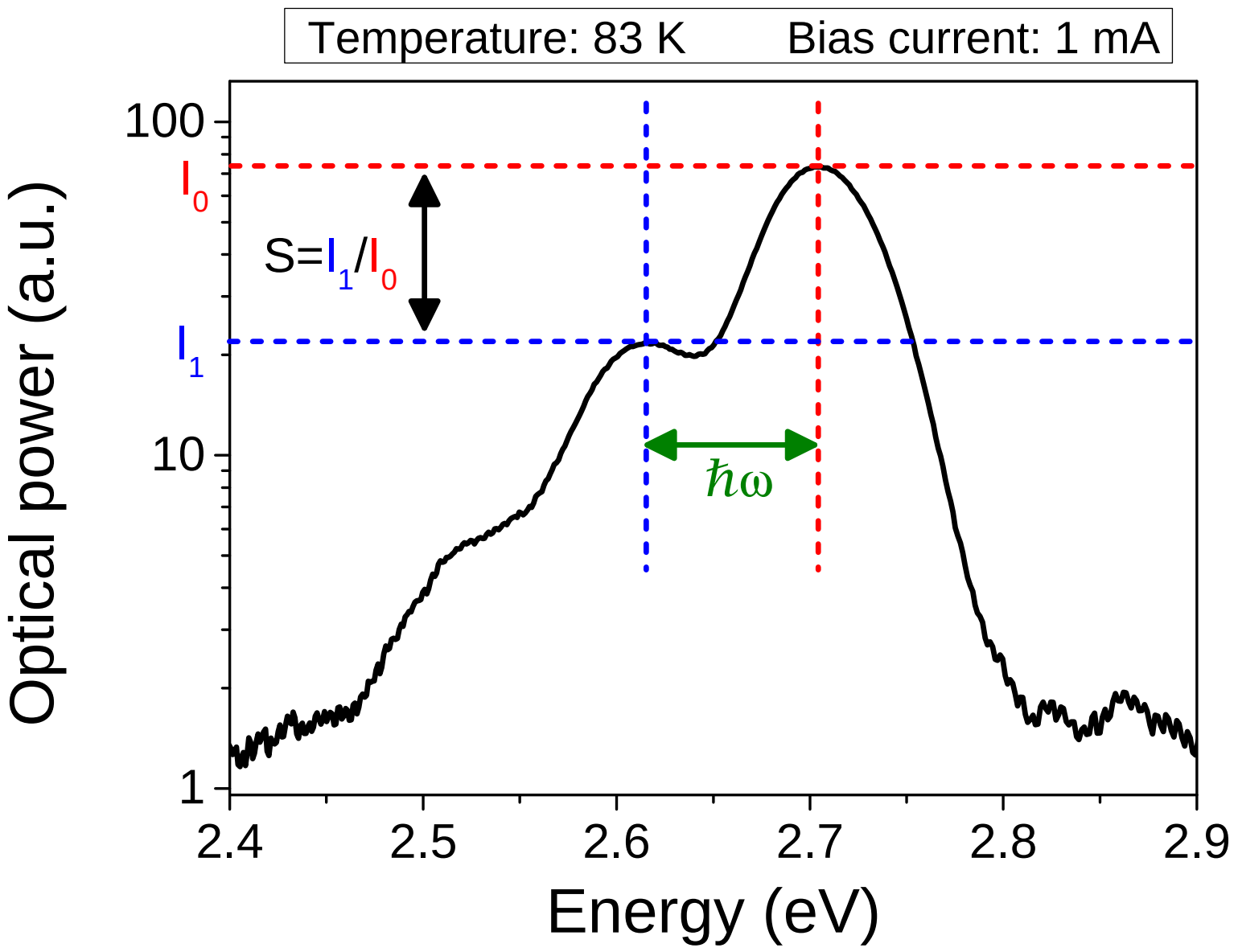
Temperature: 83 K
Bias current: 1 mA
100
10
1
I_0
I_1
S=I_1/I_0
$\hbar\omega$
Optical power (a.u.)
2.4
2.5
2.6
2.7
2.8
2.9
Energy (eV)

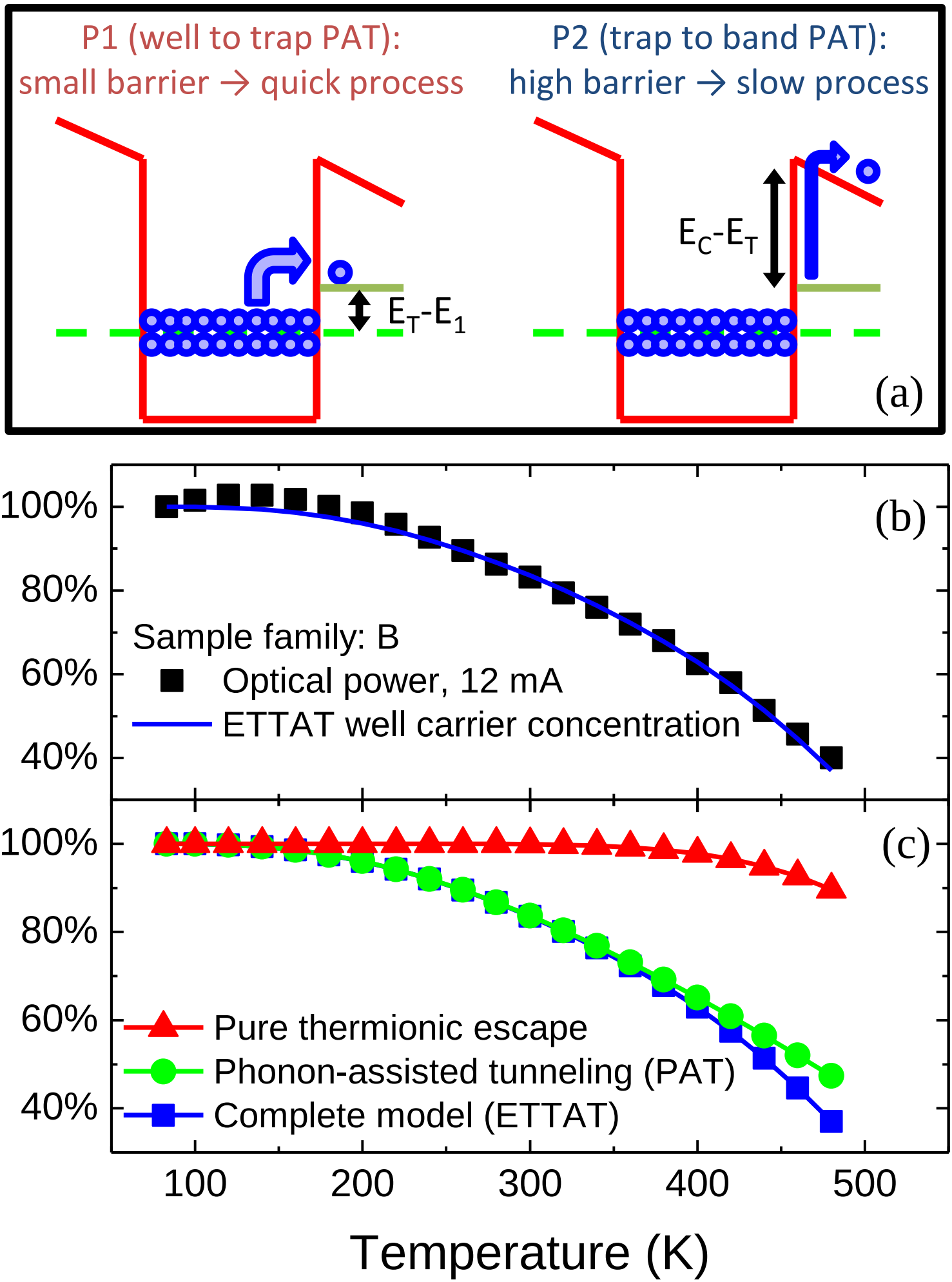
P1 (well to trap PAT):
small barrier → quick process
P2 (trap to band PAT):
high barrier → slow process
E_T-E_1
E_C-E_T
(a)
(b)
100%
80%
60%
40%
Sample family: B
Optical power, 12 mA
ETTAT well carrier concentration
(c)
Pure thermionic escape
Phonon-assisted tunneling (PAT)
Complete model (ETTAT)
100
200
300
400
500
Temperature (K)

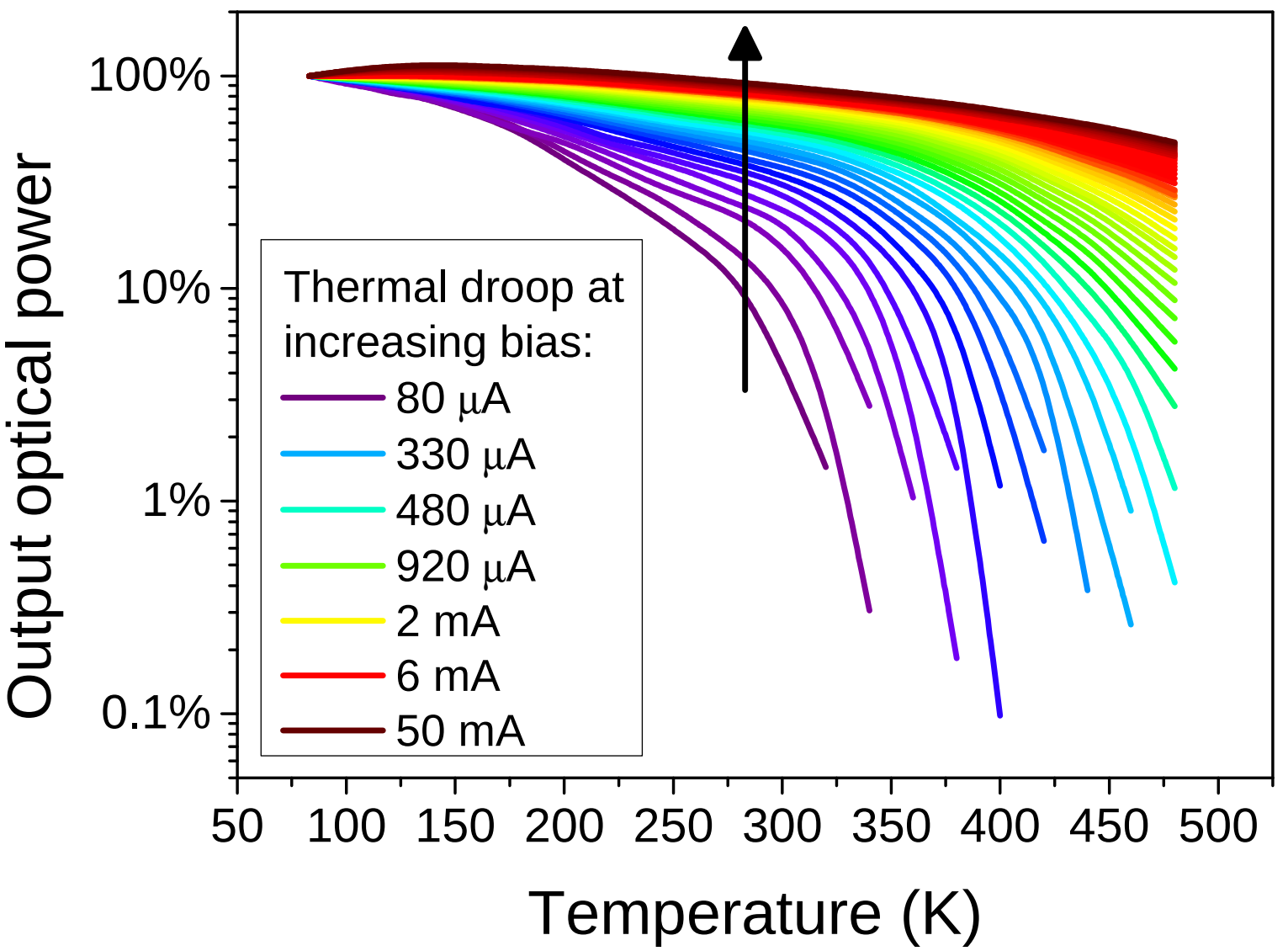
Output optical power
100%
10%
1%
0.1%
50
100
150
200
250
300
350
400
450
500
Temperature (K)
Thermal droop at increasing bias:
80 μA
330 μA
480 μA
920 μA
2 mA
6 mA
50 mA